NEURAL SPACE MAPPING OPTIMIZATION FOR EM-BASED DESIGN

Mohamed H. Bakr, *Student Member*, *IEEE,* John W. Bandler, *Fellow*, *IEEE,*
Mostafa A. Ismail, *Student Member*, *IEEE*, José E. Rayas-Sánchez, *Senior Member*, *IEEE,*
and Qi-Jun Zhang, *Senior Member*, *IEEE*

Abstract   We propose, for the first time, Neural Space Mapping (NSM) optimization for EM-based design. NSM optimization exploits our Space Mapping-based neuromodeling techniques to efficiently approximate the mapping. A novel procedure that does not require troublesome parameter extraction to predict the next point is proposed. The initial mapping is established by performing upfront fine model analyses at a reduced number of base points. Coarse model sensitivities are exploited to select those base points. Huber optimization is used to train, without testing points, simple SM-based neuromodels at each NSM iteration. The technique is illustrated by a high-temperature superconducting (HTS) quarter-wave parallel coupled-line microstrip filter and a bandstop microstrip filter with quarter-wave resonant open stubs.

I. INTRODUCTION

Artificial Neural Networks (ANNs) are suitable models for microwave circuit yield optimization and statistical design [1, 2]. Neuromodels are computationally much more efficient than EM or physical

models and can be more accurate than empirical, physics-based models. Once they are trained with reliable learning data, obtained by either EM simulation or by measurement, the neuromodel can be used for efficient and accurate optimization within the region of training. This has been the conventional approach to optimization of microwave structures using ANNs [3].

The principal drawback of this ANN optimization approach is the cost of generating sufficient learning samples, since the simulations/measurements must be performed for many combinations of different values of geometrical, material, process and input signal parameters over a large region. Additionally, it is well known that the extrapolation ability of neuromodels is poor, making unreliable any solution predicted outside the training region. Introducing knowledge, as in [4], can alleviate these limitations.

A powerful new method for optimization of microwave circuits based on Space Mapping (SM) technology and Artificial Neural Networks (ANN) is presented. An innovative strategy is proposed to exploit the SM-based neuromodeling techniques [5] in an efficient Neural Space Mapping (NSM) optimization algorithm, including frequency. NSM requires a reduced set of upfront learning base points. A "coarse" or empirical model is used not only as source of knowledge that reduces the amount of learning data and improves the generalization performance of the SM-based neuromodel, but also as a means to select the initial learning base points through sensitivity analysis. A novel procedure that does not require troublesome parameter extraction to predict the next point is presented. Huber optimization is used to train the SM-based neuromodels at each iteration. The SM-based neuromodels are developed without using testing points: their generalization performance is controlled by gradually increasing their complexity starting with a 3-layer perceptron with 0 hidden neurons. NSM optimization is illustrated by a high-temperature superconducting (HTS) quarter-wave parallel coupled-line microstrip filter and a bandstop microstrip filter with quarter-wave resonant open stubs.

II. SPACE MAPPING CONCEPT INCLUDING FREQUENCY

Space Mapping (SM) is a powerful concept for circuit design and optimization that combines the

computational efficiency of "coarse" models with the accuracy of "fine" models. The coarse models are typically equivalent circuit models, which are computationally very efficient but often have a limited validity range for their parameters, beyond which the simulation results may become inaccurate. On the other hand, fine models can be provided by an electromagnetic (EM) simulator, or even by direct measurements: they are very accurate but CPU intensive. SM establishes a mathematical link between the coarse and the fine models. It directs the bulk of CPU intensive evaluations to the coarse model, while preserving the accuracy and confidence offered by the fine model. The SM technique was originally developed by Bandler *et al.* [6].

In the Space Mapping technique with frequency dependence, the operating frequency ω is also included in the mapping function. This allows us to simulate the coarse model at a different frequency ω_c.

Let the vectors x_c and x_f represent the design parameters of the coarse and fine models, respectively, and $R_c(x_c, \omega_c)$ and $R_f(x_f, \omega)$ the corresponding model responses (for example, R_c and R_f might contain the real and imaginary parts of S_{21}). R_c is much faster to calculate but less accurate than R_f.

The aim of Space Mapping optimization, including frequency, is to find an appropriate mapping P from the fine model input space to the coarse model input space

$$\begin{bmatrix} x_c \\ \omega_c \end{bmatrix} = P(x_f, \omega) \tag{1}$$

such that

$$R_c(x_c, \omega_c) \approx R_f(x_f, \omega) \tag{2}$$

Once a mapping P valid in the region of interest is found, the coarse model can be used for fast and accurate simulations in that region.

III. NEURAL SPACE MAPPING (NSM) OPTIMIZATION: AN OVERVIEW

Fig. 1 shows the flow diagram of NSM optimization. Here we explain the overall operation of NSM optimization; a detailed description of the main blocks is presented in the following sections.

We start by finding the optimal solution x_c^* that yields the desired response using the coarse model. We select $2n$ additional points following an n-dimensional star distribution [5, 7] centered at x_c^*, as shown in Fig. 2, where n is the number of design parameters ($x_c, x_f \in \Re^n$). The percentage of deviation from x_c^* for each design parameter is determined according to the coarse model sensitivities. The larger the sensitivity of the coarse model response w.r.t. a certain parameter, the smaller the percentage of variation of that parameter. We assume that the coarse model sensitivities are similar to those of the fine model.

The fine model response R_f at the optimal coarse model solution x_c^* is then calculated. If R_f is approximately equal to the desired response, the algorithm ends, otherwise we develop an SM-based neuromodel over the $2n+1$ fine model points.

Once an SM-based neuromodel with small learning errors is available, *we use it as an improved coarse model*, optimizing its parameters to generate the desired response. The solution to this optimization problem becomes the next point in the fine model parameter space, and it is included in the learning set.

We calculate the fine model response at the new point, and compare it with the desired response. If it is still different, we re-train the SM-based neuromodel over the extended set of learning samples and the algorithm continues. If not, the algorithm terminates.

IV. COARSE OPTIMIZATION

During the coarse optimization phase of NSM optimization, we want to find the optimal coarse model solution x_c^* that generates the desired response over the frequency range of interest. The vector of coarse model responses R_c might contain m different responses of the circuit,

$$\boldsymbol{R}_c(\boldsymbol{x}_c) = [\boldsymbol{R}_c^1(\boldsymbol{x}_c)^T \quad \cdots \quad \boldsymbol{R}_c^m(\boldsymbol{x}_c)^T]^T \tag{3}$$

where each individual response has been sampled at F_p frequency points,

$$\boldsymbol{R}_c^r(\boldsymbol{x}_c) = [R_c^r(\boldsymbol{x}_c, \omega_1) \quad \cdots \quad R_c^r(\boldsymbol{x}_c, \omega_{F_p})]^T, \quad r = 1, \ldots, m \tag{4}$$

The desired response $\boldsymbol{R}^*$ is expressed in terms of specifications. The problem of circuit design using the coarse model can be formulated as [8]

$$\boldsymbol{x}_c^* = \arg \min_{\boldsymbol{x}_c} U(\boldsymbol{R}_c(\boldsymbol{x}_c)) \tag{5}$$

where U is a suitable objective function. For example, U could be a minimax objective function expressed in terms of upper and lower specifications for each response and frequency sample. A rich collection of objective functions, for different design constraints, is formulated by Bandler *et al.* in [8].

V. TRAINING THE SM-BASED NEUROMODEL DURING NSM OPTIMIZATION

At the ith iteration, we want to find the simplest neuromapping $\boldsymbol{P}^{(i)}$ such that the coarse model using that mapping approximates the fine model at all the learning points. This is realized by solving the optimization problem

$$\boldsymbol{w}^* = \arg \min_{\boldsymbol{w}} \left\| [\cdots \quad \boldsymbol{e}_s^T \quad \cdots]^T \right\| \tag{6}$$

with

$$\boldsymbol{e}_s = \boldsymbol{R}_f(\boldsymbol{x}_f^{(l)}, \omega_j) - \boldsymbol{R}_c(\boldsymbol{x}_{c_j}^{(l)}, \omega_{c_j}), \tag{7a}$$

$$\begin{bmatrix} \boldsymbol{x}_{c_j}^{(l)} \\ \omega_{c_j} \end{bmatrix} = \boldsymbol{P}^{(i)}(\boldsymbol{x}_f^{(l)}, \omega_j, \boldsymbol{w}) \tag{7b}$$

$$j = 1, \ldots, F_p \tag{7c}$$

$$l = 1, \ldots, 2n + i \tag{7d}$$

$$s = j + F_p(l - 1) \tag{7e}$$

where $2n + i$ is the number of training base points for the input design parameters and F_p is the number of

frequency points per frequency sweep. It is seen that the total number of learning samples at the ith iteration is $s = (2n + i) F_p$.

(7b) is the input-output relationship of the ANN that implements the mapping at the ith iteration. Vector $\boldsymbol{w}$ contains the internal parameters (weights, bias, etc.) of the ANN. The paradigm chosen to implement $\boldsymbol{P}$ is a 3-layer perceptron.

All the SM-based neuromodeling techniques proposed in [5] can be exploited to efficiently solve (6). In the Space Mapped Neuromodeling (SMN) approach only the design parameters are mapped, as illustrated in Fig. 3, and both models use the same frequency:

$$\begin{bmatrix} \boldsymbol{x}_{c_j}^{(l)} \\ \omega_{c_j} \end{bmatrix} = \boldsymbol{P}^{(i)}(\boldsymbol{x}_f^{(l)}, \omega_j, \boldsymbol{w}) = \begin{bmatrix} \boldsymbol{P}_{SM}^{(i)}(\boldsymbol{x}_f^{(l)}, \boldsymbol{w}) \\ \omega_j \end{bmatrix} \tag{8}$$

In the Frequency-Dependent Space Mapped Neuromodeling (FDSMN) approach, illustrated in Fig. 4, both coarse and fine models are simulated at the same frequency, but the mapping from the fine to the coarse parameter space is dependent on the frequency:

$$\begin{bmatrix} \boldsymbol{x}_{c_j}^{(l)} \\ \omega_{c_j} \end{bmatrix} = \boldsymbol{P}^{(i)}(\boldsymbol{x}_f^{(l)}, \omega_j, \boldsymbol{w}) = \begin{bmatrix} \boldsymbol{P}_{FDSM}^{(i)}(\boldsymbol{x}_f^{(l)}, \omega_j, \boldsymbol{w}) \\ \omega_j \end{bmatrix} \tag{9}$$

The Frequency Space Mapped Neuromodeling (FSMN) technique (see Fig. 5) establishes a mapping not only for the design parameters but also for the frequency variable, such that the coarse model is simulated at a different frequency to match the fine model response:

$$\begin{bmatrix} \boldsymbol{x}_{c_j}^{(l)} \\ \omega_{c_j} \end{bmatrix} = \boldsymbol{P}^{(i)}(\boldsymbol{x}_f^{(l)}, \omega_j, \boldsymbol{w}) = \begin{bmatrix} \boldsymbol{P}_{FSM}^{(i)}(\boldsymbol{x}_f^{(l)}, \omega_j, \boldsymbol{w}) \end{bmatrix} \tag{10}$$

For those cases where the shapes of the fine and coarse model responses are nearly identical but shifted in frequency, the Frequency Mapped Neuromodeling technique (see Fig. 6) simulates the coarse model with the same physical parameters used by the fine model, but at a different frequency to align both responses:

$$\begin{bmatrix} x_{c_j}^{(l)} \\ \omega_{c_j} \end{bmatrix} = \boldsymbol{P}^{(i)}(x_f^{(l)}, \omega_j, \boldsymbol{w}) = \begin{bmatrix} x_f^{(l)} \\ P_{FM}^{(i)}(x_f^{(l)}, \omega_j, \boldsymbol{w}) \end{bmatrix} \tag{11}$$

Finally, the Frequency Partial-Space Mapped Neuromodeling (FPSMN) technique maps only some of the design parameters and the frequency (see Fig. 7), making an even more efficient use of the implicit knowledge in the coarse model:

$$\begin{bmatrix} x_{c_j}^{(l)} \\ \omega_{c_j} \end{bmatrix} = \boldsymbol{P}^{(i)}(x_f^{(l)}, \omega_j, \boldsymbol{w}) = \begin{bmatrix} \overset{\bullet}{x}_f^{(l)} \\ \overset{\bullet}{x}_{c_j}^{(l)} \\ \omega_{c_j} \end{bmatrix} = \begin{bmatrix} \overset{\bullet}{x}_f^{(l)} \\ P_{FPSM}^{(i)}(x_f^{(l)}, \omega_j, \boldsymbol{w}) \end{bmatrix} \tag{12}$$

Note that the "design" parameters of the coarse model do not change with frequency only in the SMN and FM neuromappings.

The starting point for the first training process is a unit mapping, i.e., $\boldsymbol{P}^{(0)}(x_f^{(l)}, \omega_j, \boldsymbol{w}_u) = [x_f^{(l)T} \ \omega_j]^T$, for $j = 1,\ldots, F_p$ and $l = 1,\ldots, 2n+1$, where $\boldsymbol{w}_u$ contains the internal parameters of the ANN that give a unit mapping. The SM-based neuromodel is trained in the next iterations using the previous mapping as the starting point.

The complexity of the ANN (the number of hidden neurons and the SM-based neuromodeling technique) is gradually increased according to the learning error ε_L, starting with a linear mapping (3-layer perceptron with 0 hidden neurons). In other words, we use the simplest ANN that yields an acceptable learning error ε_L, defined as

$$\varepsilon_L = \left\| [\cdots \ \boldsymbol{e}_s^T \ \cdots]^T \right\| \tag{13}$$

where $\boldsymbol{e}_s$ is obtained from (7) using the current optimal values for the ANN internal parameters $\boldsymbol{w}^*$.

In our implementation, the neuromapping for the first iteration is approximated using the FMN technique, so that any possible severe misalignment in frequency between the coarse and the fine model responses is first alleviated. Then, the physical parameters are gradually mapped, following a FPSMN technique.

Linear Adaptive Frequency-Space Mapping (LAFSM) is a special case of NSM optimization,

corresponding to the situation when the number of hidden neurons of the ANN is zero at all iterations.

VI. SM-BASED NEUROMODEL OPTIMIZATION

At the ith iteration of NSM optimization, we use an SM-based neuromodel with small learning error as an improved coarse model, optimizing its parameters to generate the desired response. We denote the SM-based neuromodel response as $\boldsymbol{R}_{SMBN}$, defined as

$$\boldsymbol{R}_{SMBN}(\boldsymbol{x}_f) = [\boldsymbol{R}^1_{SMBN}(\boldsymbol{x}_f)^T \quad \dots \quad \boldsymbol{R}^m_{SMBN}(\boldsymbol{x}_f)^T]^T \tag{14}$$

where

$$\boldsymbol{R}^r_{SMBN}(\boldsymbol{x}_f) = [R^r_c(\boldsymbol{x}_{c1}, \omega_{c1}) \quad \dots \quad R^r_c(\boldsymbol{x}_{cF_p}, \omega_{cF_p})]^T, \quad r = 1,\dots,m \tag{15}$$

with

$$\begin{bmatrix} \boldsymbol{x}_{c_j} \\ \omega_{c_j} \end{bmatrix} = \boldsymbol{P}^{(i)}(\boldsymbol{x}_f, \omega_j, \boldsymbol{w}^*) \tag{16}$$

$$j = 1,\dots,F_p \tag{17}$$

The solution to the following optimization problem becomes the next iterate:

$$\boldsymbol{x}_f^{(2n+i+1)} = \arg \min_{\boldsymbol{x}_f} U(\boldsymbol{R}_{SMBN}(\boldsymbol{x}_f)) \tag{18}$$

with U defined as in (5). If an SMN neuromapping is used to implement $\boldsymbol{P}^{(i)}$ (see Fig. 3), the next iterate can be obtained in a simpler manner by solving

$$\boldsymbol{x}_f^{(2n+i+1)} = \arg \min_{\boldsymbol{x}_f} \left\| \boldsymbol{P}^{(i)}_{SM}(\boldsymbol{x}_f, \boldsymbol{w}^*) - \boldsymbol{x}_c^* \right\| \tag{19}$$

VII. NSM ALGORITHM

Step 0.   Find $\boldsymbol{x}_c^*$ by solving (5).

Step 1.   Choose $\boldsymbol{x}_f^{(1)},\dots, \boldsymbol{x}_f^{(2n)}$ following a star distribution around $\boldsymbol{x}_c^*$.

Step 2.   Initialize $i = 1$, $\boldsymbol{x}_f^{(2n+i)} = \boldsymbol{x}_c^*$.

Step 3.   Stop if $\left\| \boldsymbol{R}_f (\boldsymbol{x}_f{}^{(2n+i)}, \omega_j) - \boldsymbol{R}_c(\boldsymbol{x}_c^*, \omega_j) \right\| \leq \varepsilon_R$, $j = 1, \ldots, F_p$.

Step 4.   Initialize $\boldsymbol{P}^{(i)} = \boldsymbol{P}^{(i-1)}$, where

$$\boldsymbol{P}^{(0)}(\boldsymbol{x}_f{}^{(l)}, \omega_j, \boldsymbol{w}_u) = \begin{bmatrix} \boldsymbol{x}_f{}^{(l)} \\ \omega_j \end{bmatrix}, \quad j = 1, \ldots, F_p; \quad l = 1, \ldots, 2n+i.$$

Step 5.   Find $\boldsymbol{w}^*$ by solving (6).

Step 6.   Calculate ε_L using (13).

Step 7.   If $\varepsilon_L > \varepsilon_{\min}$, increase the complexity of $\boldsymbol{P}^{(i)}$ and go to Step 5.

Step 8.   If an SM neuromapping is used to implement $\boldsymbol{P}^{(i)}$, solve (19),

otherwise solve (18).

Step 9.   Set $i = i + 1$; go to Step 3.

VIII. HTS MICROSTRIP FILTER

We apply NSM optimization to a high-temperature superconducting (HTS) quarter-wave parallel coupled-line microstrip filter [9], illustrated in Fig. 8. L_1, L_2 and L_3 are the lengths of the parallel coupled-line sections and S_1, S_2 and S_3 are the gaps between the sections. The width W is the same for all the sections as well as for the input and output microstrip lines, of length L_0. A lanthanum aluminate substrate with thickness H and dielectric constant ε_r is used.

The specifications are $|S_{21}| \geq 0.95$ in the passband and $|S_{21}| \leq 0.05$ in the stopband, where the stopband includes frequencies below 3.967 GHz and above 4.099 GHz, and the passband lies in the range [4.008GHz, 4.058GHz]. The design parameters are $\boldsymbol{x}_f = [L_1\ L_2\ L_3\ S_1\ S_2\ S_3]^T$. We take $L_0 = 50$ mil, $H = 20$ mil, $W = 7$ mil, $\varepsilon_r = 23.425$, loss tangent $= 3 \times 10^{-5}$; the metalization is considered lossless.

Sonnet's *em*™ [10] driven by Empipe™ [11] was employed as the fine model, using a high-resolution grid with a 1mil×1mil cell size. OSA90/hope™ [12] built-in linear elements MSL (microstrip line), MSCL (two-conductor symmetrical coupled microstrip lines) and OPEN (open circuit) connected

9

by circuit theory over the same MSUB (microstrip substrate definition) are taken as the "coarse" model.

The following optimal coarse model solution is found, as in [13]: $x_c^* = [188.33 \quad 197.98 \quad 188.58 \quad 21.97 \quad 99.12 \quad 111.67]^T$ (in mils). The coarse and fine model responses at the optimal coarse solution are shown in Fig. 9.

The initial $2n+1$ points are chosen by performing sensitivity analysis on the coarse model: a 3% deviation from x_c^* for L_1, L_2, and L_3 is used, while a 20% is used for S_1, S_2, and S_3. The corresponding fine and coarse model responses at these 13 star-distributed learning points are shown in Fig. 10.

Fig. 11 shows the evolution of the learning errors at the $2n+1$ points as we increase the complexity of the neuromapping during the first iteration. It is seen that mapping the frequency has a dramatic effect on the alignment of the responses, and a simple FPSM neuromapping is needed. The final mapping is implemented with a 3-layer perceptron with 7 inputs (6 design parameters and the frequency), 5 hidden neurons, and 3 output neurons (ω, L_1, and S_1).

As indicated in Step 8, we calculate the next point by optimizing the coarse model with the mapping found. The next point predicted is $x_f^{(14)} = [185.37 \quad 195.01 \quad 184.24 \quad 21.04 \quad 86.36 \quad 91.39]^T$ (in mils), which matches the desired response with excellent accuracy, as seen in Fig. 12. As a final test, both the FPSMN model and the fine model are simulated at the NSM solution $x_f^{(14)}$ using a very fine frequency sweep, with a frequency step of 0.005GHz. The NSM solution satisfies the specifications, as shown in Fig. 13. A detailed illustration of the passband using an even finer frequency sweep is shown in Fig. 14. The HTS filter is optimized in only one NSM iteration.

IX. BANDSTOP MICROSTRIP FILTER WITH OPEN STUBS

NSM optimization is applied to a bandstop microstrip filter with quarter-wave resonant open stubs, illustrated in Fig. 15. L_1, L_2 are the open stub lengths and W_1, W_2 the corresponding widths. An alumina substrate with thickness $H = 25$ mil, width $W_0 = 25$ mil and dielectric constant $\varepsilon_r = 9.4$ is used for a 50 Ω feeding line.

The specifications are $|S_{21}| \leq 0.01$ in the stopband and $|S_{21}| \geq 0.9$ in the passband, where the stopband lies between 9.3 GHz and 10.7 GHz, and the passband includes frequencies below 8 GHz and above 12 GHz. The design parameters are $x_f = [W_1 \; W_2 \; L_0 \; L_1 \; L_2]^T$.

Sonnet's *em*™ [10] driven by Empipe™ [11] was employed as the fine model, using a high-resolution grid with a 1mil×1mil cell size. As coarse model, we use simple transmission lines for modeling each microstrip section (see Fig. 16) and classical formulas [14] to calculate the characteristic impedance and the effective dielectric constant of each transmission line. It is seen that $L_{c2} = L_2 + W_0/2$, $L_{c1} = L_1 + W_0/2$, and $L_{c0} = L_0 + W_1/2 + W_2/2$. We use OSA90/hope™ [12] built-in transmission line elements TRL.

The following optimal coarse model solution is found for L_0, L_1, and L_2 of quarter-wave lengths at 10 GHz: $x_c^* = [6.00 \; 9.01 \; 106.45 \; 110.15 \; 108.81]^T$ (in mils). The coarse and fine model responses at the optimal coarse solution are shown in Fig. 17.

The initial $2n+1$ points are chosen by performing sensitivity analysis on the coarse model: a 50% deviation from x_c^* for W_1, W_2, and L_0 is used, while a 15% is used for L_1, and L_2. A simple FM neuromapping (see Fig. 6) with 2 hidden neurons (3LP:6-2-1, ω) was used to match the responses at the learning base points. The FM neuromodel and the fine model responses at the optimal coarse solution are shown in Fig. 18. Optimizing the FM neuromodel to satisfy the specifications (Step 8 of the NSM algorithm), the next iterate is $x_f^{(12)} = [6.54 \; 16.95 \; 91.26 \; 113.30 \; 120.72]^T$ (in mils). The coarse and fine model responses at this point are shown in Fig. 19.

We performed a second NSM iteration. $x_f^{(12)}$ is included in the learning base points. Now a FPSM neuromapping with 3 hidden neurons is needed to match the $2n+2$ points: only ω and W_2 are mapped (3LP:6-3-2, ω, W_2). Fig. 20 shows the FPSM neuromodel and the fine model responses at $x_f^{(12)}$. Optimizing the FPSM neuromodel, the next iterate is $x_f^{(13)} = [5.92 \; 13.54 \; 83.34 \; 114.14 \; 124.81]^T$ (in mils). The coarse and fine model responses at $x_f^{(13)}$ are shown in Fig. 21. As final test, using a fine frequency sweep, we show in Fig. 22 the fine model response at $x_f^{(13)}$ and the optimal coarse response.

The bandstop microstrip filter is optimized in two NSM iterations.

X. CONCLUSIONS

We present an innovative algorithm for EM optimization based on Space Mapping technology and Artificial Neural Networks. Neural Space Mapping (NSM) optimization exploits our SM-based neuromodeling techniques to efficiently approximate the mapping from the fine to the coarse input space. NSM does not require parameter extraction to predict the next point. An initial mapping is established by performing upfront fine model analysis at a reduced number of base points. The coarse model sensitivities are exploited to select those base points. Huber optimization is used to train simple SM-based neuromodels at each iteration. The SM-based neuromodels are developed without using testing points: their generalization performance is controlled by gradually increasing their complexity starting with a 3-layer perceptron with 0 hidden neurons. A high-temperature superconducting (HTS) quarter-wave parallel coupled-line microstrip filter and a bandstop microstrip filter with quarter-wave resonant open stubs illustrate our optimization technique.

REFERENCES

[1]   A.H. Zaabab, Q.J. Zhang and M.S. Nakhla, "A neural network modeling approach to circuit optimization and statistical design," *IEEE Trans. Microwave Theory Tech.*, vol. 43, 1995, pp. 1349-1358.

[2]   P. Burrascano, M. Dionigi, C. Fancelli and M. Mongiardo, "A neural network model for CAD and optimization of microwave filters," *IEEE MTT-S Int. Microwave Symp. Dig.* (Baltimore, MD), 1998, pp. 13-16.

[3]   P.M. Watson and K.C. Gupta, "Design and optimization of CPW circuits using EM-ANN models for CPW components," *IEEE Trans. Microwave Theory Tech.*, vol. 45, 1997, pp. 2515-2523.

[4]   P.M. Watson, G.L. Creech and K.C. Gupta, "Knowledge based EM-ANN models for the design of wide bandwidth CPW patch/slot antennas," *IEEE AP-S Int. Symp. Digest* (Orlando, FL), July 1999, pp. 2588-2591.

[5]   J.W. Bandler, M.A. Ismail, J.E. Rayas-Sánchez and Q.J. Zhang, "Neuromodeling of microwave circuits exploiting space mapping technology," *IEEE Trans. Microwave Theory Tech.*, vol. 47, 1999, pp. 2417-2427.

[6]   J.W. Bandler, R.M. Biernacki, S.H. Chen, P.A. Grobelny and R.H. Hemmers, "Space mapping technique for electromagnetic optimization," *IEEE Trans. Microwave Theory Tech.*, vol. 42,

1994, pp. 2536-2544.

[7]   R.M. Biernacki, J.W. Bandler, J. Song and Q.J. Zhang, "Efficient quadratic approximation for statistical design," *IEEE Trans. Circuit Syst*., vol. 36, 1989, pp. 1449-1454.

[8]   J.W. Bandler and S.H. Chen, "Circuit optimization: the state of the art," *IEEE Trans. Microwave Theory Tech*., vol. 36, 1988, pp. 424-443.

[9]   J.W. Bandler, R.M. Biernacki, S.H. Chen, W.J. Getsinger, P.A. Grobelny, C. Moskowitz and S.H. Talisa, "Electromagnetic design of high-temperature superconducting microwave filters," *Int. J. Microwave and Millimeter-Wave CAE*, vol. 5, 1995, pp. 331-343.

[10]   *em*™ Version 4.0b, Sonnet Software, Inc., 1020 Seventh North Street, Suite 210, Liverpool, NY 13088, 1997.

[11]   Empipe™ Version 4.0, formerly Optimization Systems Associates Inc., P.O. Box 8083, Dundas, Ontario, Canada L9H 5E7, 1997, now Agilent EEsof EDA, 1400 Fountaingrove Parkway Santa Rosa, CA 95403-1799.

[12]   OSA90/hope™ Version 4.0, formerly Optimization Systems Associates Inc., P.O. Box 8083, Dundas, Ontario, Canada L9H 5E7, 1997, now Agilent EEsof EDA, 1400 Fountaingrove Parkway, Santa Rosa, CA 95403-1799.

[13]   M.H. Bakr, J.W. Bandler, R.M. Biernacki, S.H. Chen, and K. Madsen, "A trust region aggressive space mapping algorithm for EM optimization," *IEEE Trans. Microwave Theory Tech.*, vol. 46, 1998, pp. 2412-2425.

[14]   M. Pozar, *Microwave Engineering*. Amherst, MA: John Wiley and Sons, 1998, pp. 162.

Start

COARSE OPTIMIZATION: find the optimal coarse model solution x_c^* that generates the desired response R^*

$$R_c(x_c^*) = R^*$$

Form a learning set with $B_p = 2n+1$ base points, by selecting $2n$ additional points around x_c^*, following a star distribution

Choose the coarse optimal solution as a starting point for the fine model
$$x_f = x_c^*$$

Calculate the fine response
$$R_f(x_f)$$

Include the new x_f in the learning set and increase B_p by one

End   yes

$R_f(x_f) \approx R^*$

no

Update x_f

SM BASED NEUROMODELING: Find the simplest neuromapping P such that

$$R_f(x_f^{(l)}, \omega_j) \approx R_c(P(x_f^{(l)}, \omega_j))$$

$$l = 1,..., B_p \text{ and } j = 1,..., F_p$$

SMBNM OPTIMIZATION: Find the optimal x_f such that

$$R_{SMBN}(x_f) = R_c(P(x_f)) \approx R^*$$

Fig. 1. Neural Frequency Space Mapping (NFSM) Optimization.

x_{f2}

x_{f3} x_{f1}

x_c^*
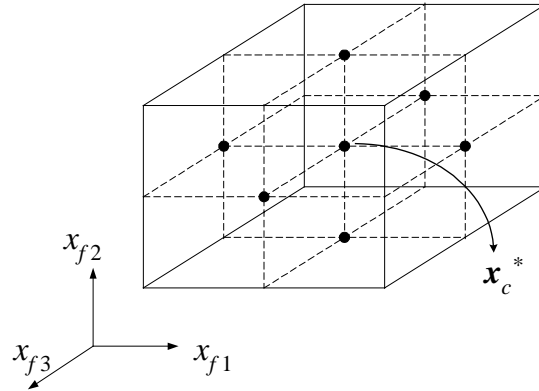
Fig. 2. Three-dimensional star distribution for the initial base points.
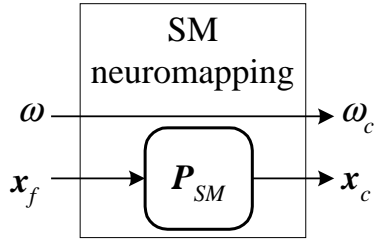
Fig. 3 . Space Mapped neuromapping.
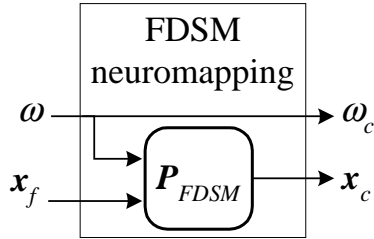
Fig. 4. Frequency-Dependent Space Mapped neuromapping.
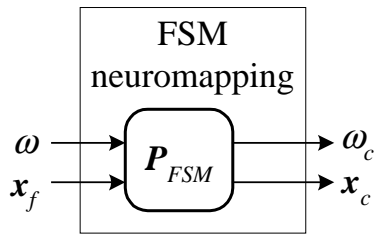
Fig. 5. Frequency Space Mapped neuromapping.
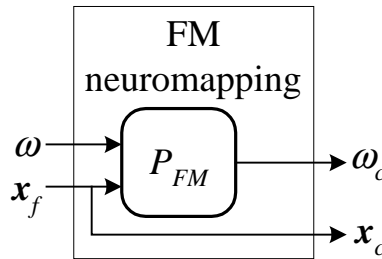
Fig. 6. Frequency Mapped neuromapping.
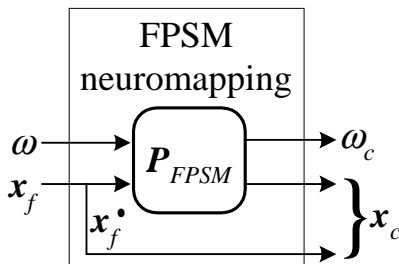
Fig. 7. Frequency Partial-Space Mapped neuromapping.
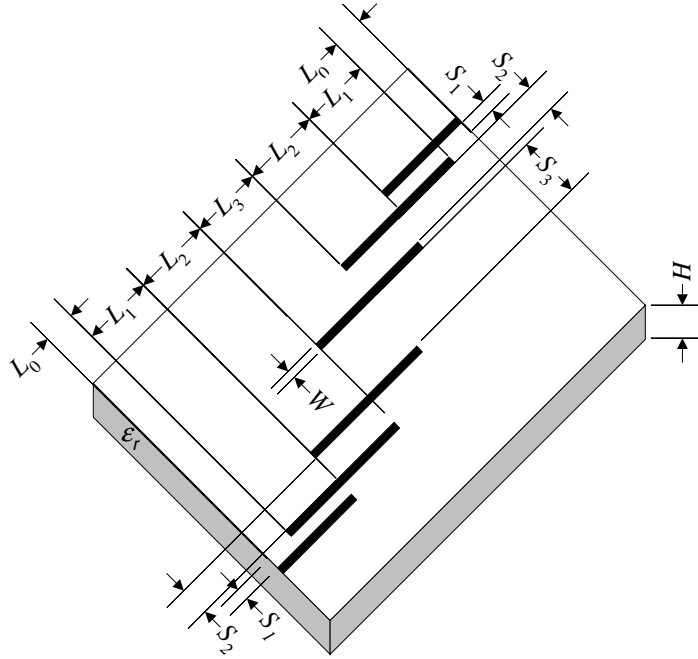
Fig. 8. HTS quarter-wave parallel coupled-line microstrip filter.
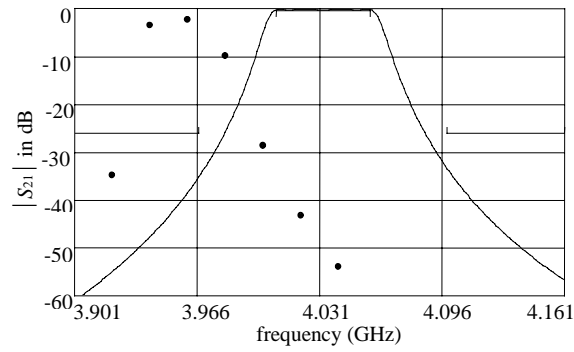
Fig. 9. Coarse and fine model responses at the optimal coarse
solution: OSA90/hope™ (−) and *em*™ (●)

(a)

(b)
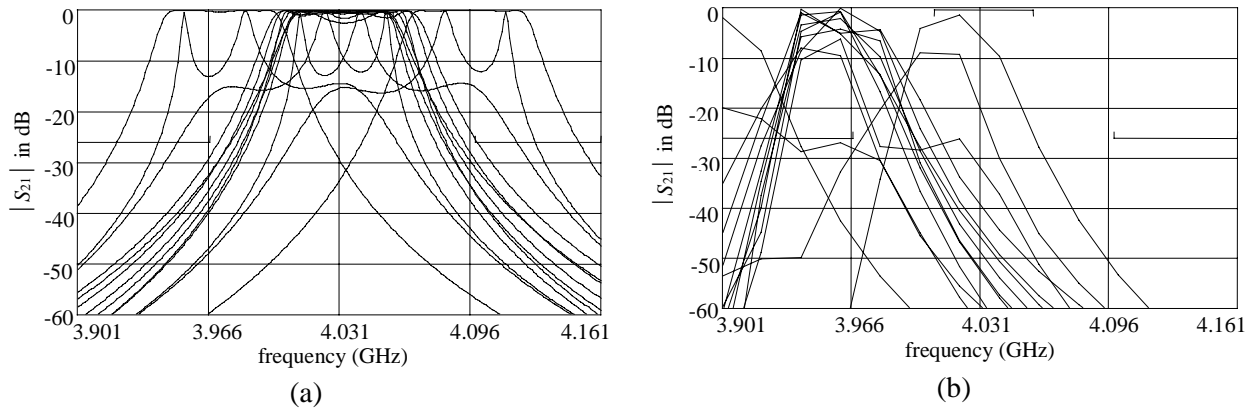
Fig. 10. Coarse and fine model responses at the initial $2n+1$ base points around
the optimal coarse solution: (a) OSA90/hope™, (b) *em*™.

16
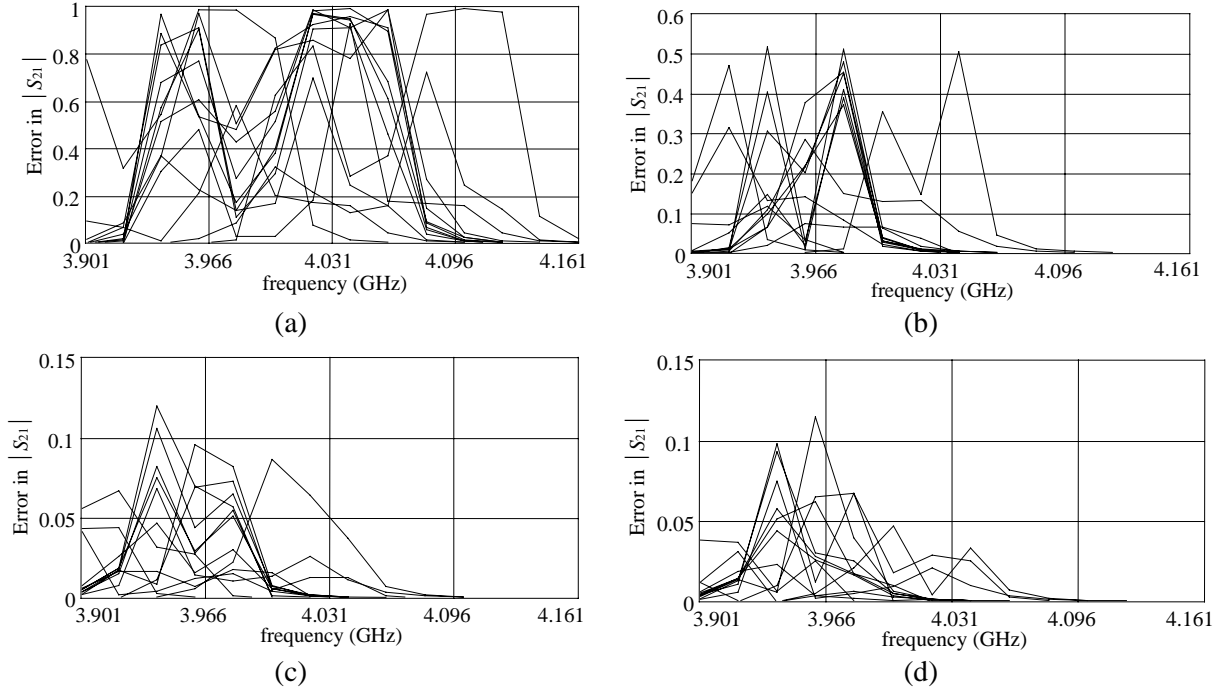
Fig. 11. Learning errors at initial base points: (a) at the starting point, (b) mapping ω
with a 3LP:7-3-1, (c) mapping ω and L_1 with a 3LP:7-4-2, and
(d) mapping ω, L_1 and S_1 with a 3LP:7-5-3.
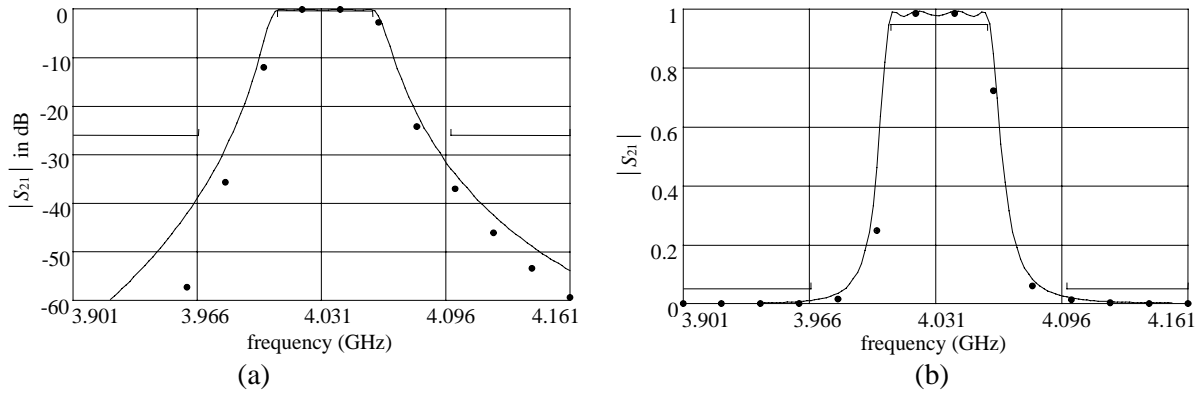
Fig. 12. *em*™ (•) and FPSM 7-5-3 (−) model responses at the next point
predicted after the first NSM iteration: (a) $|S_{21}|$ in dB, (b) $|S_{21}|$.
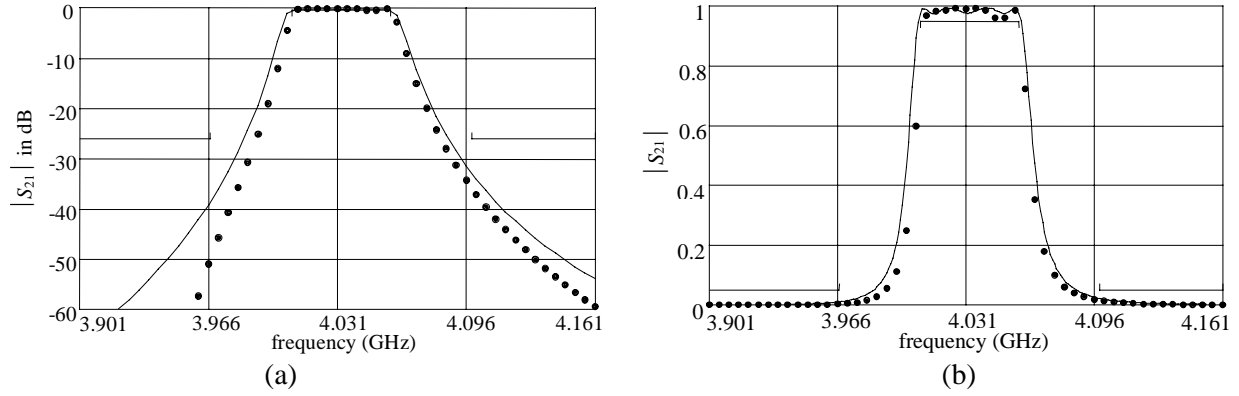
Fig. 13. *em*™ (•) and FPSMN 7-5-3 (−) model responses, using a fine frequency sweep, at the next point predicted after the first NSM iteration: (a) $|S_{21}|$ in dB, (b) $|S_{21}|$.
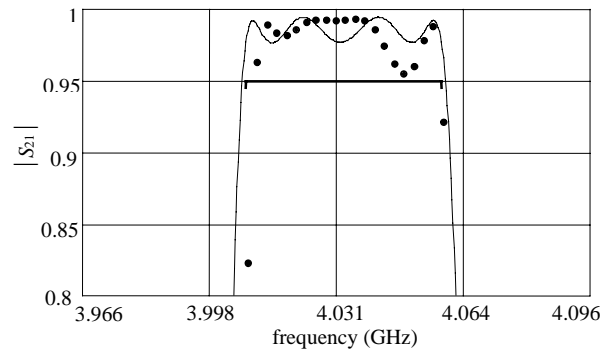
Fig. 14. *em*™ (•) and FPSMN 7-5-3 (−) model responses in the bandpass, using a fine frequency sweep, at the next point predicted after the first NSM iteration.
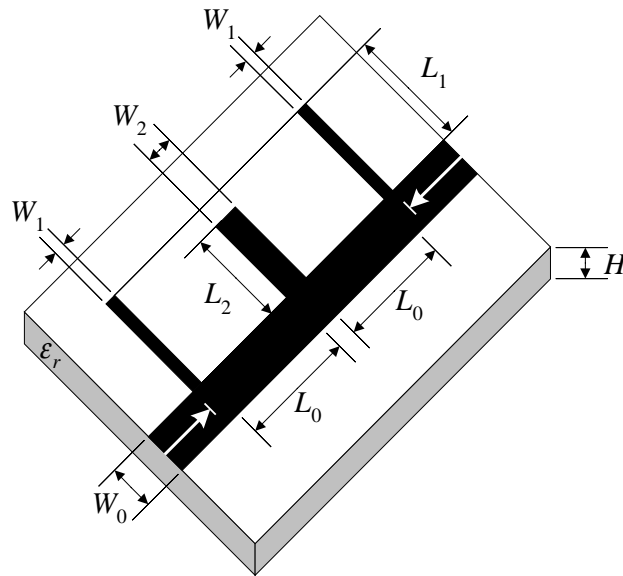
Fig. 15. Bandstop microstrip filter with quarter-wave resonant open stubs.

18
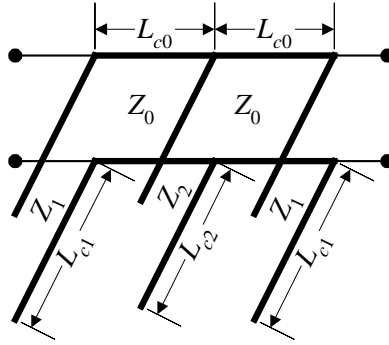
Fig. 16. Coarse model of the bandstop microstrip filter with open stubs.
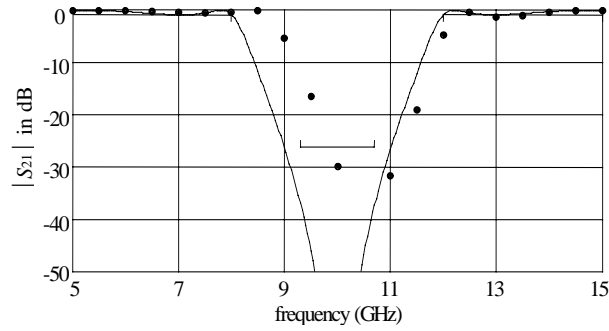
Fig. 17. Coarse and fine model responses at the optimal coarse
solution: OSA90/hope™ (−) and *em*™ (•).
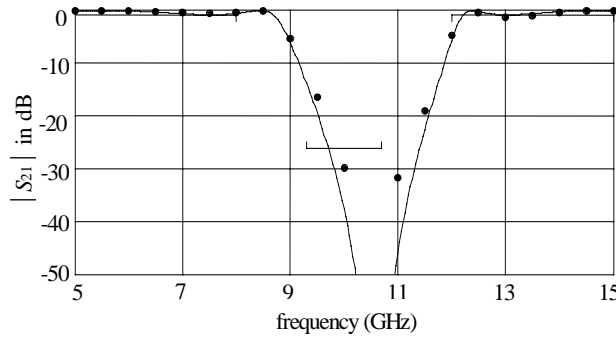
Fig. 18. FM (3LP:6-2-1, ω) neuromodel (−) and the fine model (•)
responses at the optimal coarse solution.
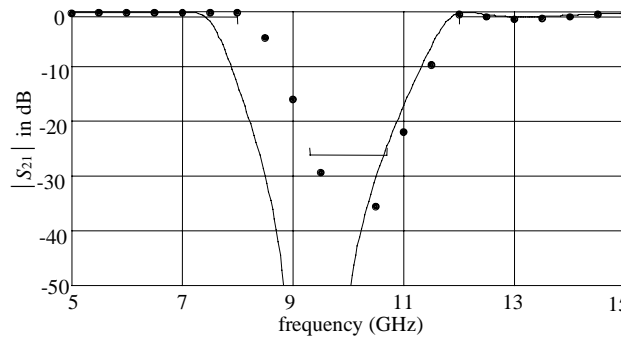
Fig. 19. Coarse (−) and fine (•) model responses at the next
point predicted by the first NSM iteration.

19
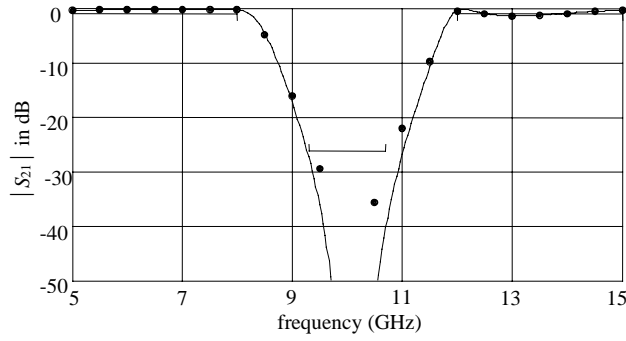
Fig. 20. FPSM (3LP:6-3-2, ω, W_2) neuromodel ($-$) and the fine model ($\bullet$) responses at the point predicted by the first NSM iteration.
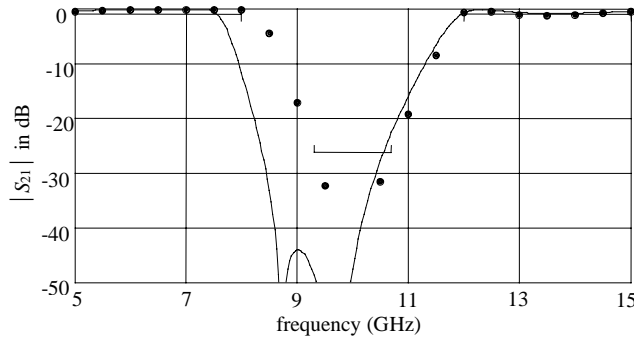
Fig. 21. Coarse ($-$) and fine model ($\bullet$) responses at the next point predicted by the second NSM iteration.
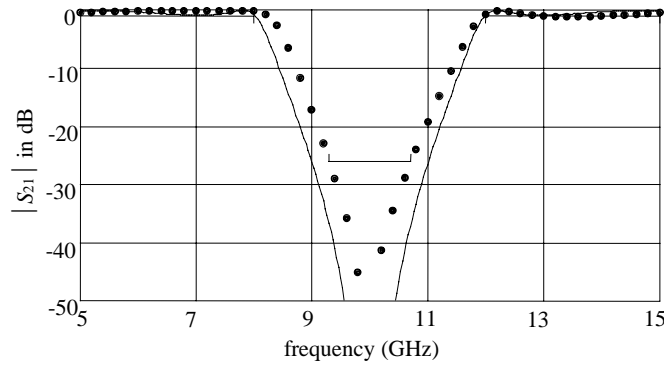
Fig. 22. Fine model response ($\bullet$) at the next point predicted by the second NSM iteration and optimal coarse response ($-$), using a fine frequency sweep.